Translation Of Laser-Based Three-Dimensional Printing Technologies

Tommaso Baldacchini, Jayant Saksena, Samuel C. Sklare, Benjamin T. Vinson, Yong Huang, Douglas B. Chrisey, and Roger J. Narayan

Tommaso Baldacchini, University of California**,** Irvine, USA; tbaldacchini@gmail.com

Jayant Saksena, Tulane University, USA; jsaksena@tulane.edu

Samuel C. Sklare, Tulane University, USA; ssklare@tulane.edu

Benjamin T. Vinson, Tulane University, USA; bvinson1@tulane.edu

Yong Huang, University of Florida, USA; yongh@ufl.edu

Douglas B. Chrisey, Tulane University, USA; dchrisey@tulane.edu

Roger J. Narayan, University of North Carolina, and North Carolina State University, USA; roger_narayan@unc.edu

Laser-based three-dimensional (3D) printing methods, including laser direct-write cell printing and two-photon polymerization, have seen significant advances because of their unique photonic characteristics. Several mechanisms have been developed to increase the overall throughput of two-photon polymerization. Recent efforts to develop complex medically relevant structures using laser direct-write cell printing have also been demonstrated; for example, an *ex vivo* experimental platform for time-lapse imaging of cancer cell dynamics during angiogenesis within a microvascular network, which combines laser direct-write cell printing into the rat mesentery culture model; a model that simulates a 3D in vivo culture. Laser 3D printing methods hold significant promise for 3D printing

of tissue engineering scaffolds, microstructured medical devices, and other medically relevant structures.

Introduction

.Laser energy offers unique capabilities for processing materials since the light is monochromatic as well as temporally and spatially coherent. The high intensity and directionality of especially pulsed laser energy have allowed lasers to play a leading role in industrial applications such as welding, marking, and cutting of materials. For example, lasers have enabled cutting of micropatterned drug eluting cardiovascular stents out of metals and resorbable polymers.[4]

More recently, lasers are being used for three-dimensional (3D) printing of functional materials, in which computer-controlled laser beam processes create 3D structures (generally in a layer-by-layer manner). Researchers have made significant progress in the use of lasers for 3D printing of biomaterials via two-photon polymerization (TPP) and laser-direct-write bioprinting processes. This article describes efforts to increase the overall throughput of two-photon polymerization as well as an innovative *ex vivo* experimental platform for time-lapse imaging of cancer cell dynamics during angiogenesis within a microvascular network that utilizes laser direct-write cell printing and the rat mesentery culture model.

Throughput of 3D fabrication by two-photon polymerization

Among the tools available for the fabrication of microstructures, TPP exhibits a series of unique and useful characteristics.[5–11] Among 3D printing processes, TPP is the only technique that can achieve “true” 3D writing, that is, the realization of complex objects without the need for a layer-by-layer approach. Furthermore, it can perform laser direct laser writing with the highest precision enabling feature sizes as small as 100 nm in a relatively straightforward manner.

When compared with competitive technologies, TPP is highly attractive for the realization of 3D microstructures because of the excellent reproduction fidelity. While microstereolithography, laser sintering, and inkjet printing allow layer-by-layer 3D writing, they are not capable of depositing materials with

dimensions smaller than a few micrometers.[12–14] Alternatively, lithographic processes with the highest writing resolution such as electron-beam lithography are limited to the fabrication of essentially two-dimensional (2D) microstructures.[15] It is not surprising that TPP has evolved in recent years from a technique employed by laser specialists to a tool that is used by scientists and engineers in many research fields;[16,17] and tremendous results have been obtained in the realization of optical elements such as photonic crystals, cloaking devices, and complex lens assemblies.[18–20] Mechanical metamaterials with remarkable performances have been produced; in addition, remotely driven machines have been fabricated within microfluidic channels.[21,22] Moreover, TPP has had a significant influence in biomedical applications where both microdevices and scaffolds for cell culture have been manufactured and successfully tested.[23]

Several researchers have demonstrated the processing of tissue engineering scaffolds using TPP. Koroleva et al. used TPP to create 3D Zr-Si scaffolds with 150-, 200-, and 250-μm pore sizes for bone-tissue engineering.[10] The TPP-produced scaffolds were seeded with human bone marrow stem cells and human adipose tissue-derived stem cells; the scaffolds were then cultured for three weeks in osteoinductive and control media; osteoinductive media facilitates the differentiation of osteoprogenitor cells to osteoblasts, which support the formation of new bone. **Figure 1** shows high magnification images that reveal calcium phosphate deposition by bone marrow stem cells and human adipose tissue-derived stem cells in both osteogenic (Figure 1a–b and Figure 1c–d) and control (Figure 1e–f and Figure 1g–h) media. Figure 1i–l show EDX mapping data, which indicates the presence of calcium and phosphorus on the scaffolds. The 150-μm pore size Zr-Si scaffolds showed the strongest level of matrix mineralization, as confirmed by calcium deposition. Cells were shown to adhere to the lateral surfaces of the scaffolds and fill the pore spaces. The cellular matrix density appeared to be greater for both cell types on scaffolds with the 150-μm pore size. Cells cultured on scaffolds with larger pores showed fewer cell-to-cell contacts. This study concludes that TPP-manufactured Zr-Si scaffolds may have use in scaffolds for bone-tissue engineering.

In another study, Nguyen et al. demonstrated TPP of polyethylene glycol diacrylate scaffolds with microscale features (e.g., tissue engineering scaffolds) using a photoinitiator containing riboflavin and triethanolamine. TPP using the riboflavin-triethanolamine mixture showed lower photosensitivity than Irgacure 2959 and Irgacure 369, two commercially available photoinitiators. The comet assay, which detects breaks in the deoxyribonucleic acid (DNA) strands, indicated that materials polymerized with riboflavin-triethanolamine caused less damaged to the DNA than those polymerized with Irgacure 369 or Irgacure 2959. The growth of bovine aortic endothelial cells on a TPP-fabricated polyethylene glycol diacrylate scaffold that was made using a riboflavin–triethanolamine photoinitiator was demonstrated; a LIVE/DEAD stain on the scaffold five days after seeding showed a significant number of live cells and only a few dead cells (**Figure 2**). The cells entered the 100-μm pores and showed normal morphology. This study indicated that riboflavin is a biocompatible and water-soluble photoinitiator for TPP of tissue engineering scaffolds and other medically relevant structures.

Medical devices have also been processed using TPP. For example, a hollow microneedle was created out of a biocompatible acrylate-based polymer; the microneedle was integrated with a microfluidic device that moved fluid through a 870-mm wide channel to a 3D porous carbon ion-selective electrode (**Figure 3**).[9] shows a cross-section of the K^+ ion-sensitive electrode microfluidic chip, a Solidworks drawing of K^+ ion-sensitive electrode embedded within a microfluidic device, (c) an image of the microfluidic device with the Ag/AgCl wire reference and Pt counter electrodes integrated into the fluidic channel. Scale bar = 10 mm). (d) An optical image of a single hollow microneedle that was produced using TPP. Scale bar = 250 μm). The structure allowed the hollow microneedle to distribute fluid over the three-electrode setup within the microfluidic device. The ion-sensitive electrode was responsive to physiologically relevant concentrations of potassium. This type of device may be useful for on-body detection of potassium and other physiological markers

The opportunities of TPP in the medical field will arguably only grow over time because it has the unique ability to create rationally designed 3D architectures with pore dimensions comparable to those found in many biological tissues and is becoming an enabling technology for fundamental studies of cell proliferation, differentiation, and growth by creating microscale environments with mechanical and chemical stimuli that are biologically relevant.[24,25]

There are several aspects of TPP that hinder its further use for medical applications, overall structure size and throughput have largely limited TPP to activities involving *in vitro* experiments. Other aspects need improvements also, such as repeatability between parts and consistency between machines. Furthermore, available biocompatible and biodegradable materials in TPP are still lacking. Although all these limitations are important for improving TPP, the two that render this technique impractical for biological *in vivo* applications especially include throughput time and the microscopic size of the fabricated part. Indeed, the efficiency of TPP in creating parts with dimensions ranging from millimeters to centimeters (i.e., mesoscale) with submicron spatial accuracy is still low. Even at the highest writing speeds (cm/s), fabrication times can go from a few hours to days (depending on the complexity of the structures). We next describe the state-of-the-art of TPP by focusing on the efforts to alleviate these two drawbacks, and propose steps to render TPP a manufacturing process that is more widely adopted by industry.

In TPP, near-infrared (NIR) emission is typically used to excite a photosensitive material (e.g., negative-tone resin); upon light absorption, the material polymerizes and undergoes a phase change from liquid to solid. Since the resin used in TPP is transparent to NIR light, high numerical aperture (NA) lenses and ultrashort pulsed lasers are used to enhance the probability of a multiphoton absorption event. Multiphoton absorption events involve simultaneous absorption by two or more photons by specialized molecules (e.g., photoinitiators) in the resin to commence polymerization. Multiphoton absorption only takes place in regions where light intensity is the highest; as such, polymerization is confined to a small (sub femtoliter) volume of the focused laser beam, which correlated with

the "volumetric pixel" or voxel.[26] Three-dimensional microstructures are created by precisely overlapping voxels via scanning of either the laser beam or the sample in accordance with predetermined geometries. The polymerized structures are obtained after the unsolidified part of the resin is removed with an organic solvent.

~~Recent studies have revealed that the order of optical nonlinearity in TPP depends greatly on the photoinitiator and the conditions used for light excitation.[27] Therefore, the acronym TPP is not formally correct since it describes only one of the multiphoton processes that can cause photopolymerization. Nonetheless, we will continue to refer to this high precision 3D printing technology as two-photon polymerization for simplicity (some of the other names used to describe TPP are multiphoton lithography, two-photon polymerization (2PP), multiphoton polymerization (MPP), and 3D direct laser writing).~~

The exposure curves of resins employed in TPP are quite nonlinear, thus creating a light intensity threshold below which polymerization does not occur.[28] It is the presence of this intensity threshold (I_{pol}^{th}) that permits the formation of voxels with dimensions that are considerably smaller than the wavelength of light used for fabrication. For example, by adjusting the intensity of the excitation laser barely above I_{pol}^{th}, voxels with lateral dimensions smaller than 100 nm can be obtained with a typical exposure wavelength of 800 nm.[29] Unfortunately, resins also possess a light intensity threshold (I_{damage}^{th}) above which boiling occurs. While I_{pol}^{th} depends on the characteristics of the photoinitiator employed and its concentration, I_{damage}^{th} is an intrinsic property of the monomers and oligomer mixtures that make the bulk of the resin. The ratio between I_{damage}^{th} and I_{pol}^{th} defines the writing dynamic range or processing window.[30] The dynamic range of a resin plays an important role in facilitating the writing of 3D microstructures at high speeds.

In practice, TPP is performed using a continuous point-by-point writing strategy. Because of the voxel dimensions, high precision motion systems need to

be employed. Hence, a common way to write microstructures is by using a three-axis piezo stage. Although these stages have the highest motion resolution, they are accompanied by modest scanning speeds (~100 μm/s) and travel ranges of 300 × 300 × 300 μm^3. In order to write faster (at least in the *x* and *y* dimensions), galvanometric scanning mirrors can be added with scanning speeds up to few centimeters per second. A higher writing speed can be obtained if galvanometric scanning mirrors in resonant mode are used.[31] With high NA objectives (1.3–1.4) though, the accessible field of view in this case is limited to only 200 × 200 μm^2.

A way to overcome these disadvantages is to introduce linear stages and use them to stitch together sections made by using either the scanning mirrors or the piezo stage. In this way, structures spanning several millimeters can be made. A drawback of this approach is the presence of stitching errors, which are inevitable due to the lower resolution and the accuracy of the linear stages.[32]

A different approach to perform TPP involves the use of high-performance air-bearing stages. In this scenario, patterning areas as large as 15 × 15 cm^2 are possible with writing speeds as high as 30 cm/s.[33] While the resolution, accuracy, and repeatability of these stages are adequate for TPP writing with high NA objectives, the upper speed limit that can be used when writing complex 3D objects is compromised by the production of defects that originate from the inertia of the system. Additionally, air-bearing stages require a larger and heavier framework to deliver high performance, adding complexity and cost. Finally, moving the substrate at a speed of cm/s around a fixed focused laser beam requires a sample that is solid in its prepolymerization state, thus narrowing the number of materials available for microfabrication.

TPP is a serial process and as such, is often depicted as a slow manufacturing technique. When TPP is compared to parallel processes employed in the mass-production of consumables (even of microscopic size), this contrast becomes evident. But, when TPP is compared to other direct writing techniques, the disparity between the writing speeds' efficiencies vanishes. The key factor to consider is not the absolute writing speed, but instead the number of voxels per s. TPP can reach values of voxels per second as high as 10^6 when writing speeds of

10 cm/s and voxels with radial dimensions of 100 nm are used.[34] The problem in making mesoscale parts by means of TPP is in the sheer number of voxels that need to be deposited. For instance, fabrication of a solid cube having a side 1 cm long will take many days to complete even when using the highest rate of voxels per second achieved so far (~10^6). A practical example can help illustrate this constraint. The fabrication time of a woodpile photonic crystal with a lattice constant of 2 μm, rod thickness of 50 nm, edge length of 1 mm, and containing 50 layers amounted to 2 h using a writing speed of 3 cm/s. If the same structure was fabricated again using the same parameters but this time with an edge length of 5 mm, a total of 10 days will be required. This large difference is due to the fact that fabrication time is proportional to the volume of the part.

Currently, writing speeds larger than 10 cm/s are not practical in TPP. This limitation is strictly linked to the available hardware. For instance, speeds of m/s will require prohibitive data rates as high as 10 Mbit/s. Furthermore, they will impose a degree of precision in the synchronization of the acousto-optic modulator function with the scanning mirrors that is difficult to reach. Moreover, at such high speeds, accelerations and decelerations of several hundred *g* will be reached during turning points, especially when writing complex geometries. Thus, at this moment, increasing the writing speed is not an option in order to increase the rate of voxels/s in TPP.

Despite the writing speed limitations imposed by the hardware, many efforts have been made so far to increase the overall throughput of TPP. The following reviews the strategies employed to reach this goal by shortening fabrication times and by increasing the overall volume of the fabricated part.

Shortening production times by using the shell fabrication approach

As the volume of the object to be created by TPP increases, the fabrication time grows rapidly to the point of becoming impractical. To overcome this obstacle, at least in the case of closed bulky objects, the shell fabrication approach can be used reducing fabrication times as much as two orders of magnitude.[35] In this writing method, only the shell of the microstructure is fabricated by TPP, leaving

its interior unpolymerized. After the development step, a quick UV curing is then used to complete the microstructure polymerization. The shell fabrication approach has been proved to be extremely effective. For example, the fabrication time of a lens with radius of 50 μm and focal length of 100 μm was reduced from 14.7 h to only 2.6 min.[36] The longer time was achieved with the traditional volume filling using a raster scan pattern, while the shorter time was achieved by implementing the shell fabrication approach. Because of shrinkage during polymerization, microstructures with large surfaces might deform during the UV curing step. Since the strength of a structure is proportional to the cube of its thickness, this inconvenient effect can be avoided using thicker shells.

Methods for high aspect ratios fabrication

Making tall structures by TPP is limited by two effects. The first originates from the working distance of microscope objectives. Working distances of high numerical objectives typically used in TPP are smaller than 200 μm. The second impediment originates from the mismatch between the index of refractions of the cover glass and of the resin. Spherical aberrations caused by this effect make it arduous to have constant axial writing accuracy when moving deeper and deeper into the resin. The combination of these two phenomena restricts the height of TPP microstructures to within tens of microns. An ingenious solution to this problem was found by using the resin itself as the immersion material of high numerical aperture objectives. This method, dubbed dip-in, eliminates the need for a cover glass with the resin sandwiched between the microscope objective and the substrate. By means of dip-in TPP, microstructures extending in height several times the microscope objective working distance were produced (**Figure 4**b).[37] Moreover, spherical aberrations remain the same independently from the microstructure height.

A limitation of the dip-in writing method is that it has been applied successfully using only one resin. To render dip-in compatible with a larger number or resins, a modification of the microscope objective can be implemented where the objective, immersion oil, and cover glass move essentially as one into the resin.[38] When used in conjunction with lower magnification objectives, this

latter methodology has produced microstructures with heights of 7 mm. A novel strategy for producing microstructures with high aspect ratios was presented recently, where simultaneous spatiotemporal focusing (SSTF) of femtosecond laser pulses was employed (Figure 4a).[39] The results of this technique are impressive, where complex structures were reproduced with overall heights larger than 1 cm.. Although the dimensions of microstructures created by SSTF TPP are amongst the largest obtained so far, SSTF writing velocity is limited by the low repetition rate of the laser employed. The processing time of the terra-cotta warrior was indeed 15 h. Furthermore, its ability to make fine feature sizes is limited.

Chemical methods for improving writing speeds

The highest writing speed currently achievable in TPP is on the order of cm/s. When the laser beam is scanned at these velocities, larger average powers are required to maintain sustainable polymerization. This is because TPP laser powers are proportional to the square root of the writing velocities. Under these experimental conditions, even small fluctuations in scanning speed or laser power can drive parasitic nonlinear optical processes with the consequence of creating micro explosions in the resin. For high-speed TPP writing, it is desirable to employ resins with large dynamic ranges. Using a resin with a large dynamic range also has the benefit of creating voxels with a wider choice of dimensions. Since the origin of I_{damage}^{th} is not yet fully understood, the most common approach to widen the dynamic range has been to lower I_{pol}^{th} by implementing efficient TPP photoinitiators. While the efficiency of these molecules depends on several factors such as the radical quantum yield and the reactivity of the active species, most efforts have been made in synthesizing, characterizing, and using molecules with large two-photon cross sections.[40] These studies have shown the benefit of using resins with large dynamic ranges. For example, the fabrication of complex microstructures was demonstrated at a writing speed of 8 cm/s by using a rationally designed photoinitiator with a two photon cross section at 800 nm of 200 cm^4s/photon (Figure 4c).[41] Another method to lower I_{pol}^{th} is to alter the

chemistry of the polymerization process. This approach has been confirmed in the case of resins made of acrylic monomers where the addition of multifunctional thiols brought a series of writing advantages among which the capability of making TPP microstructures with higher critical speeds.[42]

Replication of microstructures by molding

For TPP samples that do not possess complex 3D geometries such as micro-lenses or nano-patterns, for cells motility studies, replication by molding is an attractive method to increase fabrication throughput.[43] In this method, a master structure is first created by TPP. A mold of the master is then realized using the elastomer polydimethylsiloxane (PDMS). The mold is finally used to stamp replicas that are identical to the master structure by means of faster production processes such as UV curing. The rate at which TPP structures are produced can grow quite rapidly using this molding technique. Several molds can be made from a master structure, and each mold can be used tens of times before showing signs of material failure. Besides augmenting fabrication throughput, replication by molding offers the possibility to transfer materials that are not accessible by TPP such as ceramic slurries and highly doped resins.

Other medical structures such as solid microneedle arrays for transdermal drug delivery have been demonstrated using a combination of TPP and micromolding. **Figure 5** shows scanning electron micrographs of photoreactive acrylate-based polymer microneedle arrays created using TPP and PDMS micromolding.[6] These solid microneedles, with nominal heights of 500 μm, 750 μm, and 1000 μm, were investigated for transdermal treatment of a parasitic condition that affects people in the developing work called cutaneous leishmaniasis.[7] The microneedles were used to treat female BALB/c mice infected with either the parasite *Leishmania mexicana***,** which causes New World cutaneous leishmaniasis, or the parasite *Leishmania major*, which causes Old World cutaneous leishmaniasis. A topical dimethyl sulfoxide solution of the anti-leishmanial drug amphotericin B was applied to leishmaniasis lesions at a dose of 25 mg/kg for 10 consecutive days, either with or without preapplication of the microneedle arrays. In mice infected with *L. Mexicana*, the lesions developed

more slowly; for this infection, the nodule area was significantly less at the end of the experiment in groups receiving topical amphotericin B after application of microneedle arrays with three different lengths (500, 750, and 1000 μM nominal length) compared to the group receiving topical amphotericin B in the absence of the microneedle array treatment. In mice infected with *L. Major*, the lesions developed rapidly; for this infection, there was no difference in lesion size between groups receiving topical amphotericin B at 25 mg/kg either with or without the preapplication of microneedle arrays with 750 μM nominal length. These experiments highlight the potential of TPP-fabricated microneedle arrays as a therapy for cutaneous leishmaniasis for animal models that exhibit moderate lesions.

Application of a novel writing strategy

A hardware solution for the fast fabrication of large complex 3D microstructures using TPP does not exist thus far. On one hand, air-bearing stages are an optimal choice for precise 3D writing because of high resolution, accuracy, repeatability, and total travel range. Nonetheless, high speeds can be exploited with these stages only when outlining simple geometries. On the other hand, a move and mark procedure can be used to process areas larger than the microscope objective field of view by implementing galvanometric mirrors and linear stages. Unfortunately, this approach can exhibit stitching errors where individual sections written with the scanning mirrors do not align with each other. A different writing strategy has been recently applied to TPP to overcome this drawback. In this approach, named infinite field of view (IFOV) fabrication, the motion of the scanning mirrors is synchronized with the motion of the linear stages.[44] Thus, the information used to write a specific pattern is split in a motion commands sequence between the scanning mirrors and the linear stages. The mirrors are used for complex motions where large accelerations are unavoidable; the stages are used to maintain the sample within the objective field of view. IFOV fabrication by means of TPP has the potential to realize large structures without stitching at velocities reaching several cm/s. Initial results are encouraging--using a high numerical aperture

objective, a suspended chain mail spanning a length of 500 μm was fabricated using 1 cm/s writing speed and radial and axial hatching of 0.3 μm. Using a lower numerical aperture objective, a 3D scaffold with an overall size of 1.5 mm was fabricated in less than an hour. In both cases, because of IFOV fabrication, smooth structures with no signs of stitching errors were created.

Serial to parallel processes

TPP is a serial manufacturing process; parts are made one at a time. An obvious way to increase throughput would be to transform TPP into a parallel manufacturing process. The first attempt in this direction was achieved using a microlens array (MLA). In this method, the original laser beam is split into several laser spots, all of which are then used for TPP. Thus, a large number of microstructures can be fabricated simultaneously. In one of the first uses of MLA in TPP, 700 micro-coils were fabricated in parallel.[44] Although the implementation of MLA has demonstrated the benefit of parallel writing for TPP, the lack of flexibility limits its applications. With MLA, since the multi-foci pattern is fixed, only structures with a fixed period can be made.

A more practical approach to achieve parallel manufacturing by TPP is to use a spatial light modulator (SLM).[45] In this method, a femtosecond laser beam is divided into multiple beams by phase modulation. The main advantage of using a SLM for TPP is that the design of the multi-beam pattern can be varied by using different computer-generated hologram patterns. Thus, the implementation of an SLM device is an effective and flexible method to parallelize the TPP process; the number of laser foci and the distance/position among them are addressable in a dynamic fashion.

Figure 6 shows tissue engineering scaffolds made by TPP with single focus fabrication (Figure 6a) and four foci fabrication (Figure 6b).[45] The scaffold processed using multiple foci showed a similar morphology to the scaffold that was processed using a single focus. An image of GM-7373 bovine endothelial cells growing on a 1.6-mm scaffold made by multibeam TPP, stained with Calcein AM, and imaged with a fluorescence microscope is shown in Figure 6c.[45]

The scaffold that was processed with multiple foci showed a high cell density and a high number of viable cells.

In another study, the simultaneous fabrication of three, seven, and sixteen hemispherical microlenses was demonstrated with different spatial arrangements.[46] The fabrication time required to make these patterns helps to appreciate the speed advantage brought by using this method; the time required to make one of the microlenses is 20 min. Thus, it would take more than 5 h to produce the 16 microlenses array. Using the SLM instead, the time to make the entire array was identical to the time to make only one micro-l ens providing a massive improvement in fabrication speed. In a recent article, the authors demonstrated a printing rate of 10^7 voxel·s^{-1} by implementing a diffraction optical element (DOE) to perform TPP with an array of laser foci.[47] Besides the improvement in the printing rate, this work also demonstrates the maturing of TPP as a 3D printing process; the DOE used in this study was indeed printed using TPP. In a sense, this is a case in which the machine was used to improve itself. Parallelization of TPP has also been demonstrated by using SSTF in a projection-based system with a micromirror array.[48]

While TPP advances in writing capabilities and applications have been nothing short than remarkable, this 3D direct laser writing process has not yet crossed the barrier from being a productive tool in academic research to a viable manufacturing process. Repeatability of the manufactured parts' properties within the entire build volume, and between builds is a condition without which industrial production cannot occur. In this regard, TPP data is still lacking. It would be useful then to add *in situ* diagnostics and real-time control of TPP writing parameters to eliminate defects and increase fabrication consistency. Although some strategies have been proposed and tested to add this dimension, much more needs to be done in order to apply the concept of "certify-as-you-build" to TPP.[49]

For biological and medical applications, TPP is not yet mature enough for clinical translation. One of its limitations is the dependence on the materials

employed. In spite of the demonstrated nontoxicity of several bulk polymers used in TPP, the resins used during photopolymerization and the solvent in the post-development step are still not compatible with biological environments. Hence, either extensive post-processing washing and drying processes need to be utilized (which could deteriorate the integrity of the fabricated structure) or novel materials ought to be developed. Another limitation is the overall throughput. As discussed earlier, several approaches have been developed to overcome both the slow fabrication time and the limited dimensions of the fabricated parts in TPP. The two solutions that hold the largest promise are the use of SLM and synchronization between scanning mirrors and linear stage. Even with the implementation of these technological advances, TPP will still not be practical for the fabrication of medical devices or 3D scaffolds with dimensions that span several centimeters. In these circumstances, it will make more sense to use a combination of 3D printing processes such as stereolithography or laser direct-write cell printing with TPP.[50] While the first processes can be used to rapidly make the bulk of a part, TPP can be used to add fine features.

Cell-by-cell assembly using 3D bioprinting for preclinical targeted therapeutics

Three-dimensional printing has been applied to print mammalian cells in order to generate biological tissue constructs both as a new methodology as well as a step towards printing complete functional organs.[51] While functional organ printing is currently not yet realized, promising initial studies have demonstrated successful printing of 3D cell culture models and simple tissue constructs. As such, bioprinting is an extension of traditional 3D printing with the ultimate goal of producing living, vascularized epithelial and connective tissue and eventually whole organs for use in medical procedures, drug testing, and other disparate applications, such as healthcare training.[52]

In reality, the sheer cellular complexity of native tissues makes idealized 3D bioprinting extremely difficult; however, its goals and methods could provide the ability to produce patient-specific engineered tissue constructs using autologous cells for personalized/precision medicine applications at the cellular

level. Fabricating 3D autologous tissue constructs with complete fidelity will only be possible with a bioprinting technique that has single cell resolution. Moreover, much like the properties pertaining to tissue development, pathology, and pharmacological response differ for cells growing as 2D monolayers in petri dishes versus 3D aggregates/spheroids and organoids, tissue constructs that do not accurately replicate natural tissues will also behave differently, thereby diminishing their physiological relevance.[53] Understanding the aforementioned differences will require a bioprinting technique that can build tissue cell-by-cell. While there is still a long way to go before we can bioprint viable and fully functional autologous organs for human transplantation in a clinical setting, understanding the complexity of living and replicating diseased tissue at the cellular level is a critical first step in the process.[54]

Three-dimensional bioprinting is inherently multidisciplinary in nature—involving scientists and engineers in the fields of biology, materials science, chemistry, physics, and computer science. While its development is accelerating rapidly, it is important to be realistic in our expectations because, as stated previously, the level of cellular complexity in human tissue makes its replication extremely difficult—an example being the tumor microenvironment, which is illustrated in **Figure 7**.[55] Any sort of clinical translation will require a multidisciplinary effort to tackle the disparate issues facing bioprinting. The incremental advances in basic understanding and future applications should not be overstated as is often the case with many novel technologies; however, there is strong consensus that the future of medicine will include 3D bioprinting.[56–58] In this context, single cell-by-cell assembly will be important for understanding tissue responses and how to best exploit them therapeutically.

The recognized need to incorporate multiscale complexity in tissue models has motivated the development of biomimetic 3D culture systems,[53] *ex vivo* tissue explant models such as patient derived xenografts,[59] as well as "organ-on-a-chip" microphysiological systems.[60] None of the current models, however, enable simultaneous investigation of cancer cell migration and angiogenesis in intact microvascular networks—a requirement that more closely reflects an *in vivo* scenario. In order to develop preclinical novel targeted therapeutics for disparate diseases, we need to understand the mechanisms driving diseased tissue behavior in a model that mimics the complexity of the tissue microenvironment (e.g., cancer cells in the tumor microenvironment). We have used laser-direct-write technology to print single cancer cells or groups of cancer cells in a spatially defined manner onto *ex vivo* sections of viable mammalian tissue containing blood vessels, a lymphatic network, and representative mesenchymal stromal cells.[58,59] By doing so, we have combined the progress of a novel tissue culture model with our customized laser direct-write method for cell-by-cell assembly to create a more accurate cellular niche. This, in turn, enables real-time investigation of cellular behavior (e.g., cancer cell migration, proliferation, fate, and functionality), all while residing in a natural three-dimensional microenvironment with the striking feature of the mesentery tissue being microvascular network growth, including the formation of lymphatic vessels from pre-existing lymphatic vessels in a method believed to be similar to angiogenesis

Despite recent advances in imaging techniques to track cell movement in animal models, such as the use of optically transparent transgenic zebrafish or installation

of anatomic viewing windows for high-resolution intravital microscopy, the ability to localize distinct groups of cancer cells proximal to vessels and follow individual cell infiltration in 3D tissue culture remains elusive—illustrating the gap between current *in vivo* and traditional *in vitro* models.

In an attempt to bridge this gap, we have developed an *ex vivo* experimental platform that enables time-lapse imaging of cancer cell dynamics during angiogenesis within a real microvascular network scenario by combining two novel approaches—laser direct-write cell printing and the rat mesentery culture model.[61,62] It has been shown that the rat mesentery culture model is advantageous because it can be used for (1) real-time imaging in the same tissue, (2) quantification of endothelial cell sprouting at specific locations within a microvascular network during growth factor-induced angiogenesis, and (3) investigating functional effects of multi-functional vascular smooth muscle on endothelial sprouting.[63] We have also shown that lymphatic vessels in our model maintain their lymphatic identity and can be induced to undergo lymphangiogenesis.

A key advantage of this model is its simplicity (i.e., the tissue is easy to obtain, self-contained, and does not need to be embedded). The mesentery's thinness (20–40 μm) allows for observation of intact networks down to a single cell level and makes it an ideal tissue for printing exogenous cells. Using laser-direct-write printing technology (**Figure 8**), human breast cancer cells and fibroblasts were deposited in spatially defined patterns onto the vascularized rat mesentery tissue. After printing, cells remained viable, proliferative, and migratory. Our results demonstrate, for the first time, cell printing onto live tissues for tracking short-term cancer cell dynamics within intact microvascular networks. Heterogeneous cell printing, quantification of cancer cell influence on

angiogenesis, and observation of cancer cell integration into blood and lymphatic vessels support the feasibility of making specific spatial and temporal measurements, which are not possible in other *in vitro* systems. We envision this new *ex vivo* model platform will enable high content investigation of cancer cell behavior in a real tissue environment and future studies focused on the systematic probing of reciprocal cellular interactions between cancer cells, fibroblasts, blood vessels, and lymphatic vessels.

Triple-negative MDA-MB-231 breast cancer cells[1] were successfully printed using laser direct-writing onto an *ex vivo* mesentery tissue (Figure 8). The real-time imaging coincident with the laser direct-write system allowed for the selection of the area on the mesentery tissue for printing. Ejecting a single droplet of cell suspension established a local group of adherent MDA-MB-231 cells on the mesentery tissue. After 1 h of incubation, a combination of round and spindle-shaped cellular morphologies indicated various states of cell attachment.

To demonstrate the deposition of cells into spatially defined pattern positions, additional groups of cancer cells were printed to form 4 × 4 matrix arrays of 16 spots (0.8 mm center-to-center spot spacing, print area 16 mm^2) (**Figure 9**). Cells were printed onto microvascular networks containing blood and lymphatic vessels. Blood versus lymphatic vessel identity was distinguishable by relative diameter, vessel morphology, and lectin or PECAM fluorescence labeling intensity. Lymphatic identity based on these features is supported by previous co-labeling of lymphatic vessels with lectin or PECAM and typical lymphatic markers such as LYVE-1, Prox1, and podoplanin. Arterioles, venules, and capillaries were identified by position in the network, vessel morphology, and the fluorescence intensity. Following printing, MDA-MB-231 cells attached to the tissue substrate and maintained their initially deposited positions. Cells displayed adherent morphology 2 h after bioprinting. The average spot diameter was 401 μm, and the average number of cells per spot was 40 (n = 8 completed arrays, over two batches). Interactions between cancer cells and microvascular networks are shown in **Figure 10**. MDA-MB-231 cells interacted with the PECAM-positive endothelial cells, and integrated into the micro-vessels[61].

The novel combination of the laser direct-write bioprinting technology and the rat mesentery culture model enabled the spatial patterning of single cells, cell clusters, and heterogeneous cell populations onto intact microvascular networks containing blood vessels and lymphatic vessels. The *ex vivo* platform provided the capability for quantification of cancer cell dynamics and effects within a biologically relevant tissue environment at temporal and spatial resolutions not possible with other models (i.e., between the MDA-MB-231 cells with both blood and lymphatic vessels) (Figure 10). Sub-0.5 μm confocal images supported the observation of interactions between MDA-MB-231 cells and PECAM-positive endothelial cells. Cells were also observed to be capable of interacting with the PECAM-positive endothelial cells of micro-vessels. While invasive MDA-MB-231 breast cancer cells were used as the model cell line to demonstrate the feasibility of this model, the laser-direct-write bioprinting process is cell type-independent. In addition to the MDA-MB-231 cells, we also demonstrated the ability to print MCF-7 breast cancer cells and fibroblasts[61]. The ability to print heterogeneous cell groups could allow for the generation of intra-tumor patterns to study fibroblast-directed events, cancer cell type-dependent behavior, and collective cell migration.

This *ex vivo* model platform should motivate future studies focused on the systematic probing of the reciprocal cellular interactions between cancer cells, fibroblasts, blood vessels, and lymphatic vessels (e.g., the ability to distinguish or evaluate breast cancer subtypes), which at the molecular level are characterized by unique signaling as well as genomic, transcriptomic, metabolomic and epigenomic signatures that define their phenotype. The ability to answer such questions within one model supports the potential for this cancer cell-microvascular network model to be an intermediary platform between whole organisms and reductionist monolayer assays. It has also been recently demonstrated that the *ex vivo* mesentery tissue can be perfused to incorporate flow effects, thereby increasing this model's physiological relevance.[64] Future envisioned applications could include utilizing patient-derived tumor cells or other specific cell populations implicated in the cancer microenvironment for

preclinical and personalized drug screening strategies through elucidation of cellular interactions.

Future outlook

Several technological limitations must be overcome for laser-based 3D printing technologies and other 3D printing technologies to achieve translation to widespread use in commercial manufacturing and clinical medicine. J. Slotwinski has described the following technical challenges in the field of 3D printing: (1) understanding materials properties, (2) obtaining design-allowable material data, (3) preparing feedstock materials, (4) acquiring a better understanding of 3D printing processes, (5) enhancing the surface finish (e.g., decreasing the roughness) of 3D printing-produced structures, (7) increasing the 3D printing processing rate, (8) increasing the sizes of structures that can be produced by 3D printing, and (9) improving the data formats used with 3D printing to facilitate translation of patient imaging data to information that can be used to create a patient-specific structure.[65]

M. Di Prima with the US Food and Drug Administration considered four material-centric parameters that provide limitations to current 3D printing-produced medical devices: (1) mechanical properties, (2) physical properties, and (3) sterility.[66] He noted that 3D printing-produced polymers may exhibit much lower tensile strength in the build direction than in the perpendicular direction to the build direction. Pore-shaped artifacts of the 3D printing process or intentionally included pores may reduce mechanical strength of 3D printing-produced structures. Removing excess material (e.g., support structures or excess precursor material) from 3D printing-produced structures, particularly engineered porous surfaces, may sometimes be difficult. Finally, sterilizing or removing contamination from devices with complex shapes that are created via 3D printing may present challenges. The bioprinting field is faced with unique limitations, including (a) processing rates that are too low to print large cell-seeded tissues, and (b) damage to the cells and other biological materials during storage or printing. [67] It is anticipated that sustained efforts by researchers in academia,

government, and industry will be needed to overcome these challenges over the coming years.

Acknowledgments

T.B. acknowledges financial support from the NSF under Grant No. CMMI-1905582.

References

1. A. McWilliams, *Global Markets and Technologies for Medical Lasers* (BCC Research, Wellesley, MA, 2017).

2. K. Parkhi, *Global Markets for Laser Systems, Components, and Materials* (BCC Research, Wellesley, MA, 2020).

3. T.H. Maiman, *Nature* **187**, 493 (1960).

4. L. Chen, *Proc. Int. Congr. Appl. Lasers Electro-optics (ICALEO)* (2008) p. 320.

5. A. Ovsianikov, B. Chichkov, P. Mente, N.A. Monteiro-Riviere, A. Doraiswamy, R.J. Narayan, *Int. J. Appl. Ceram. Technol.* **4**, 22 (2007).

6. S.D. Gittard, A. Ovsianikov, N.A. Monteiro-Riviere, J. Lusk, P. Morel, P. Minghetti, C. Lenardi, B.N. Chichkov, R.J. Narayan, *J. Diabetes Sci. Technol.* **3**, 304 (2009).

7. A.K. Nguyen, K. Yang, K. Bryant, J. Li, A.C. Joice, K.A. Werbovetz, R.J. Narayan, *Biomed. Microdev.* **21**, 8 (2019).

8. A.K. Nguyen, S.D. Gittard, A. Koroleva, S. Schlie, A. Gaidukeviciute, B.N. Chichkov, R.J. Narayan, *Regen. Med.* **8**, 725 (2013).

9. P.R. Miller, X. Xiao, I. Brener, D.B. Burckel, R. Narayan, R. Polsky, *Adv. Healthcare Mater.* **3**, 876 (2014).

10. A. Koroleva, A. Deiwick, A. Nguyen, S. Schlie-Wolter, R. Narayan, P. Timashev, V. Popov, V. Bagratashvili, B. Chichkov, *PLoS One* **10**, e011816 (2015).

11. C.N. LaFratta, J.T. Fourkas, T. Baldachini, R.A. Farrer, *Angew. Chem. Int. Ed.* **46**, 6238 (2007).

12. A. Bertsch, H. Lorenz, P. Renaud, *Sensor Actuator* **73**, 14 (1999).

13. D.D. Gu, W. Meiners, K. Wissenbach, R. Poprawe, *Int. Mater. Rev.* **57**, 133 (2012).

14. P. Calvert, *Chem. Mater.* **13**, 3299 (2001).

15. Y.F. Chen, *Microelectron. Eng.* **135**, 57 (2015).

16. T. Baldacchini (Ed.), *Three-Dimensional Microfabrication Using Two-Photon Polymerization, Fundamentals, Technology, and Applications* (Elsevier, New York, NY, William Andrew, 2016).

17. J. Stampfl, R, Liska, A. Ovsianikov (Eds.), *Multiphoton Lithography: Techniques, Materials, and Applications* (Wiley-VCH, 2016).

18. C.M. Soukoulis, M. Wegener, *Nat. Photonics* **5**, 523 (2011).

19. T. Ergin, N. Stenger, P. Brenner, J.B. Pendry, M. Wegener, *Science* **328**, 337 (2010).

20. T. Gissibl, S. Thiele, A. Herkommer, H. Giessen, *Nat. Photonics* **10**, 554 (2016).

21. J. Bauer, S. Hengsbach, I. Tesari, R. Schwaiger, O. Kraft, *PNAS* **111**, 2453 (2014).

22. S. Maruo, H. Inoue, *Appl. Phys. Lett.* **89**, 144101 (2006).

23. A.K. Nguyen, R.J. Narayan, *Mater. Today* **20**, 314 (2017).

24. A. Ovsianikov, M. Malinauskas, S. Schlie, B. Chichkov, S. Gittard, R. Narayan, M. Lobler, K. Stemberg, K.-P. Schmitz, A. Haverich, *Acta Biomater.* **7**, 967 (2011).

25. P. Tayalia, C.R. Mendonca, T. Baldacchini, D.J. Mooney, E. Mazur, *Adv. Mater.* **20**, 4494 (2008).

26. S. Maruo, J.T. Fourkas, *Laser Photonics Rev.* **2**, 100 (2008).

27. N. Liaros, J.T. Fourkas, *Laser Photonics Rev.* **11**, 1700106 (2017).

28. J.T. Fourkas, in *Three-Dimensional Microfabrication Using Two-Photon Polymerization*, T. Baldacchini, Ed. (Elsevier, 2016), pp. 45–61.

29. S. Juodkazis, V. Mizeikis, K.K. Seet, M. Miwa, H. Misawa, *Nanotechnology* **16**, 846 (2005).

30. T. Baldacchini, C.N. LaFratta, R.A. Farrer, M.C. Teich, B.E.A. Saleh, M.J. Naughton, J.T. Fourkas, *Appl. Phys. Lett.* **95**, 6072 (2004).

31. B.W. Pearre, C. Michas, J.-M. Tsang, T.J. Gardner, T.M. Otchy, *Addit. Manuf.* **30**, 100887, (2019)

32. O. Stein, Y. Liu, J. Streit, J.H. Campbell, Y.F. Lu, Y. Aglitskiy, N. Petta, *Fusion Sci. Technol.* **73**, 153 (2018).

33. S. Passinger, *Two-Photon Polymerization and Application to Surface Plasmon Polaritons* (Cuvillier Verlag, Göttingen, 2008), pp. 32–38.

34. L. Jonušauskas, D. Gailevičius, T. Baravykas, S. Juodkazis, M. Malinauskas, *Proc. SPIE 3D Printed Opt. Addit. Photonic Manuf.,* A.M. Herkommer, G. von Freymann, M. Flury, Eds, **10675**, 106750D-1 (2018).

35. D.-Y. Yang, S.H. Park, T.W. Lim, H.-J. Kong, S.W. Yi, H.K. Yang, K.-S. Lee, *Appl. Phys. Lett.* **90**, 079903 (2007).

36. M. Malinauskas, A. Žukauskas, V. Purlys, K. Belazaras, A. Momot, D. Paipulas, R. Gadonas, A. Piskarskas, H. Gilbergs, A. Gaudukevičiūte, I. Sakellari, M. Farsari, S. Juodkazis, *J. Opt.* **12**, 124010 (2010).

37. T. Bückmann, N. Stenger, M. Kadiac, J. Kaschke, A. Frölich, T. Kennerknecht, C. Eberl, M. Thiel, M. Wegener, *Adv. Mater.* **24**, 2710 (2012).

38. K. Obata, A. El-Tamer, L. Koch, U. Hinze, B.N. Chichkov, *Light Sci. Appl.* **2**, e116 (2013).

39. W. Chu, Y. Tan, P. Wang J. Xu, W. Li, J. Qi, Y. Cheng, *Adv. Mater. Technol.* **3**, 1700396 (2018).

40. W. Haske, V.W. Che, J.M. Hales, W. Dong, S. Barlow, S.R. Marder, J.W. Perry, *Opt. Express* **15**, 3426 (2007).

41. Z. Li, N. Pucher, K. Cicha, J. Torgersen, S.C. Ligon, A. Ajami, W. Husinsky, A. Rosspeintner, E. Vauthey, S. Naumov, T. Scherzer, J. Stampfl, R. Liska, *Macromolecules* **46**, 352 (2013).

42. L. Jiang, W. Xiong, Y. Zhou, Y. Liu, X. Huang, D. Li, T. Baldacchini, L. Jiang, Y. Lu, *Opt. Express* **24**, 13687 (2016).

43. C.N. LaFratta, L. Li, J.T. Fourkas, *PNAS* **103**, 8589 (2006).

44. J.-I. Kato, N. Takeyasu, Y, Adachi, H.-B. Sun, S. Kawata, *Appl. Phys. Lett.* **86**, 044102 (2005).

45. S.D. Gittard, A. Nguyen, K. Obata, A. Koroleva, R.J. Narayan, B.N. Chichkov, *Biomed. Opt. Express* **2**, 3167 (2011).

46. L. Yang, A. El-Tamer, U. Hinze, J. Li, Y. Hu, W. Huang, J. Chu, B.N. Chichkov, *Opt. Lasers Eng.* **70**, 2 (2015).

47. V. Hahn, P. Kiefer, T. Frenzel, J. Qu, E. Blasco, C. Barner-Kowollik, M. Wegener, *Adv. Func. Mater.* **30**, 1907795 (2020)

48. S.K. Saha, D. Wang, V.H. Nguyen, Y. Chang, J.S. Oakdale, S.-C. Chen, *Science* **366**, 105(2019).

49. T. Baldacchini, R. Zadoyan, *Opt. Express* **18**, 19219 (2010).

50. L. Jonušauskas, S. Juodkazis, M. Malinauskas, *J. Opt.* **20**, 053001 (2018).

51. S.V Murphy, A. Atala, *Nat. Biotechnol.* **32**, 773 (2014).

52. C.L. Ventola, *P&T* **39**, 704 (2014).

53. R. Edmondson, J.J. Broglie, A.F. Adcock, L. Yang, *Assay Drug Dev. Technol.* **12**, 207 (2014).

54. B.T. Vinson, S.C. Sklare, D.B. Chrisey, *Curr. Opin. Biomed. Eng.* **2**, 14 (2017).

55. E.S. Bishop, S. Mostafa, M. Pakvasa, H.H. Luu, M.J. Lee, J.M. Wolf, G.A. Ameer, T.-C. He, R.R. Reid, *Genes Dis.* **4**, 185 (2017).

56. M.E. Prendergast, J.A. Burdick, *Adv. Mater.* **32**, 1902516 (2020):

57. M. Albanna, K.W. Binder, S.V. Murphy, J. Kim, S.A. Qasem, W. Zhao, J. Tan, I.B. El-Amin, D.D. Dice DD, J. Marco, *Green J. Sci. Rep.* **9**, 1 (2019).

58. I. Angelopoulos, M.C. Allenby, M. Lim, M. Zamorano, *Biotechnol. Bioeng.* **117**, 272 (2019).

59. A.T. Collins, S.H. Lang, *PeerJ* **11**, e5981 (2018).

60. D.E. Ingber, *Development* **145**, 10 (2018).

61. T.B. Phamduy, R.S. Sweat, M.S. Azimi, M.E. Burow, W.L. Murfee, D.B. Chrisey, *Integr. Biol.* **7**, 1068 (2016).

62. H.E. Burks, T.B. Phamduy, M.S. Azimi, J. Saksena, M.E. Burow, B.M. Collins-Burow, D.B. Chrisey, W.L. Murfee, *J. Cell. Physiol.* **231**, 2333 (2016).

63. M. Yang, P.C. Stapor, S.M. Peirce, A.M. Betancourt, W.L. Murfee, *J. Visualized Exp.* **63**, e3954 (2012).

64. J.M. Motherwell, M. Rozenblum, P.V.G. Katakam, W.L. Murfee *Tissue Eng. Part C* **25**, 447 (2019).

65. S. Siegel, "Perspectives on Additive Manufacturing," featuring speakers from the Additive Manufacturing for Government Summit.

66. M. DiPrima, "Perspectives on Post-Printing" (Public Workshop—Additive Manufacturing of Medical Devices: An Interactive Discussion on the Technical Considerations of 3D Printing, October 8, 2014).

67. B. Bidanda P.J. Bártolo, Eds., *Virtual Prototyping & Bio Manufacturing in Medical Applications* (Springer, New York, NY, 2008).

Figure captions

Figure 1. High magnification images showing calcium phosphate deposits of hASCs and hBMSCs cultured on Zr-Si scaffolds in osteogenic (a-d) and control (e-h) conditions; (i–1) EDX mapping confirming the presence of calcium and phosphor in the accumulations. (a, c, e, g) Scale bar = 60 μm. (b, d, f, h) Scale bar = 5 μm. (i) Scale bar = 50 μm. (j–1) Scale bar = 10 μm.[10]

Figure 2. Live/dead staining images of 50% PEGda-riboflavin-TEOHA scaffold that was seeded with GM7373 bovine aortic endothelial cells. Live cells appear green, and dead cells appear red. Due to autofluorescence, PEGda appears red.[8]

Figure 3. Cross-section of a K^+ ion-sensitive electrode microfluidic chip (a), K^+ ion-sensitive electrode microfluidic chip (b), image of microfluidic chip (c) with on chip reference and counter electrodes. (scale bar = 10 mm), and optical image of single hollow microneedle (d) made with two-photon lithography (scale bar = 250 μm).[9]

Figure 4. Scanning electron microscope (SEM) images of representative microstructures fabricated by two-photon polymerization (TPP) using the methodologies described in the text. (a) SEM image front view of the fabricated 2-mm height lion sculpture, which was made possible by means of simultaneous spatiotemporal focusing. Reprinted with permission from Reference 39. © 2018 Wiley. (b) Oblique-view SEM image of a mechanical metamaterial with sixfold axis on a glass substrate, which was produced by dip-in direct laser writing. Reprinted with permission from Reference 37. © 2012 Wiley. (c) Reproduction of an ancient tower fabricated at a speed of 8 cm/s using rationally designed two-photon initiators with high polymerization efficiency. Reprinted with permission from Reference 41.f©2013 American Chemical Society.

Figure 5. Scanning electron microscope images of microneedles with nominal heights of 500 μm (a), 750 μm (b), and 1000 μm (c) obtained at a stage tilt angle of 45º. The scale bars for these images are 500 μm.[7]

Figure 6. Tissue engineering scaffolds made by two-photon polymerization (TPP) with single focus structuring (a) and four foci structuring (b). Image of bovine endothelial cells growing on a scaffold made by multibeam 2PP (c).

Figure 7. By combining advantages of laser direct-write and the rat mesentery culture model, cancer cells can be spatially patterned onto intact tissues and cultured. This *ex vivo* model platform enables time-lapse quantification of cancer cell behavior in an intact microvascular network environment with blood vessels, lymphatic vessels, extracellular matrix components, and interstitial cells. Reprinted with permission from Reference 62. © 2016 from Wiley.

Figure 8. Rat mesenteric tissue windows, defined as the thin, translucent connective tissue section between artery/vein pairs feeding the small intestine, are harvested from adult rats and spread onto inverted commercially available trans-well inserts. Cells are then embedded in a gelatin-coated UV-transparent quartz "ribbon" that can be printed directly onto the tissue. A single pulse of 193-nm ArF excimer laser causes the formation of a local vapor pocket that ejects a desired amount of cells. Use of an *in situ* camera enables real-time targeting of cells. Bioprinted tissues can be cultured using normal culture conditions for at least up to five days. Reprinted with permission from Reference 62. © 2016 from Wiley.

Figure 9. (A) Spatially defined patterns of localized cell groups on mesentery tissue and single-cell printing capability. (A) 4 × 4 array pattern (center-to-center spacing, d_{spacing} = 0.8 mm) of circular "spots" of CellTracker Red (CTR)-labeled MDA-MB-231 cancer cells on vascularized mesentery tissue, imaged 2 h following laser direct write. Mesenteric arterioles (A), venules (V), and lymphatic vessels (L) were readily identifiable by lectin labeling. Reprinted with permission from Reference 61. © 2016

Oxford University Press.

Figure 10. Interactions between cancer cells and microvascular networks are shown. MDA-MB-231 cells were identified interacting and integrating with blood vessels using sub-micron confocal microscopy. Reprinted with permission from Reference 61. © 2016 Oxford University Press.

Tommaso Baldacchini is a project scientist in the chemistry department at the University of California, Irvine. He teaches physical chemistry and optics as adjunct faculty at Chapman University. He received his PhD degree in chemistry from Boston College in 2004. From 2004 to 2006, he was a postdoctoral research fellow in the division of engineering and applied sciences at Harvard University. From 2006 to 2018, he worked as a principal scientist at Newport Corporation. His research interests focus on high-resolution laser microfabrication using ultrashort pulsed lasers. Baldacchini can be reached by email at tbaldacchini@gmail.com.

Jayant Saksena is a biomedical engineering doctoral candidate and research assistant at Tulane University. He received his master's degrees in bioengineering and material- and nanoscience from the University College Dublin and Université Pierre et Marie Curie-Sorbonne, respectively. His research involves developing bioengineered systems using laser bioprinting and processing techniques to elucidate cellular dynamics in the context of cancer and other pathologies. Saksena can be reached by email at jsaksena@tulane.edu.

Benjamin T. Vinson is a doctoral candidate and research assistant at Tulane University in biomedical engineering. He received his MS degree in biology from Texas Christian University, and his BS degree in biology and neuroscience from Washington and Lee University. His research focuses on fabricating microphysiological systems via laser direct-write bioprinting. Vinson can be reached by email at bvinson1@tulane.edu.

Charlie Sklare is an engineer at Medtronic working on laser-based brain therapies. He recently graduated with an interdisciplinary PhD degree in physics and math and an MS degree in computational science. His research interests are laser-based therapies, laser based bioprinting, and laser-material interaction modeling. Sklare can be reached by email at ssklare@tulane.edu.

Yong Huang is a professor of mechanical engineering at the University of Florida. He received his PhD degree from the Georgia Institute of Technology. His current research interests include 3D printing of biological and engineering structures (using ink jetting, laser-induced forward transfer, and extrusion), precision machining, intelligent manufacturing. Huang can be reached by email at yongh@ufl.edu.

Doug Chrisey is the Jung Professor of Materials Engineering in the Physics and Engineering Physics Department at Tulane University. He received his PhD degree from the University of Virginia. His current research interests include photonic processing of electronic materials and tissue engineering. Chrisey can be reached by email at dchrisey@tulane.edu.

Roger Narayan is a professor in the Joint Department of Biomedical Engineering at the University of North Carolina and North Carolina State University. He received his PhD degree from North Carolina State University and his MD degree from Wake Forest University. He currently serves as an editorial board member for several academic journals, including as editor-in-chief of *Medical Devices & Sensors*, and associate editor of *Applied Physics Reviews*. Narayan has also edited several books, including the textbook Biomedical Materials, the handbook Materials for Medical Devices, and The Encyclopedia of Biomedical Engineering. He has previously served as director of the TMS Functional Materials Division and the ASM International Emerging Technologies Awareness Committee; he currently serves as chair of the American Ceramic Society Bioceramics Division. Narayan can be reached by email at roger_narayan@unc.edu.

[1] https://www.ncbi.nlm.nih.gov/pmc/articles/PMC3532890/

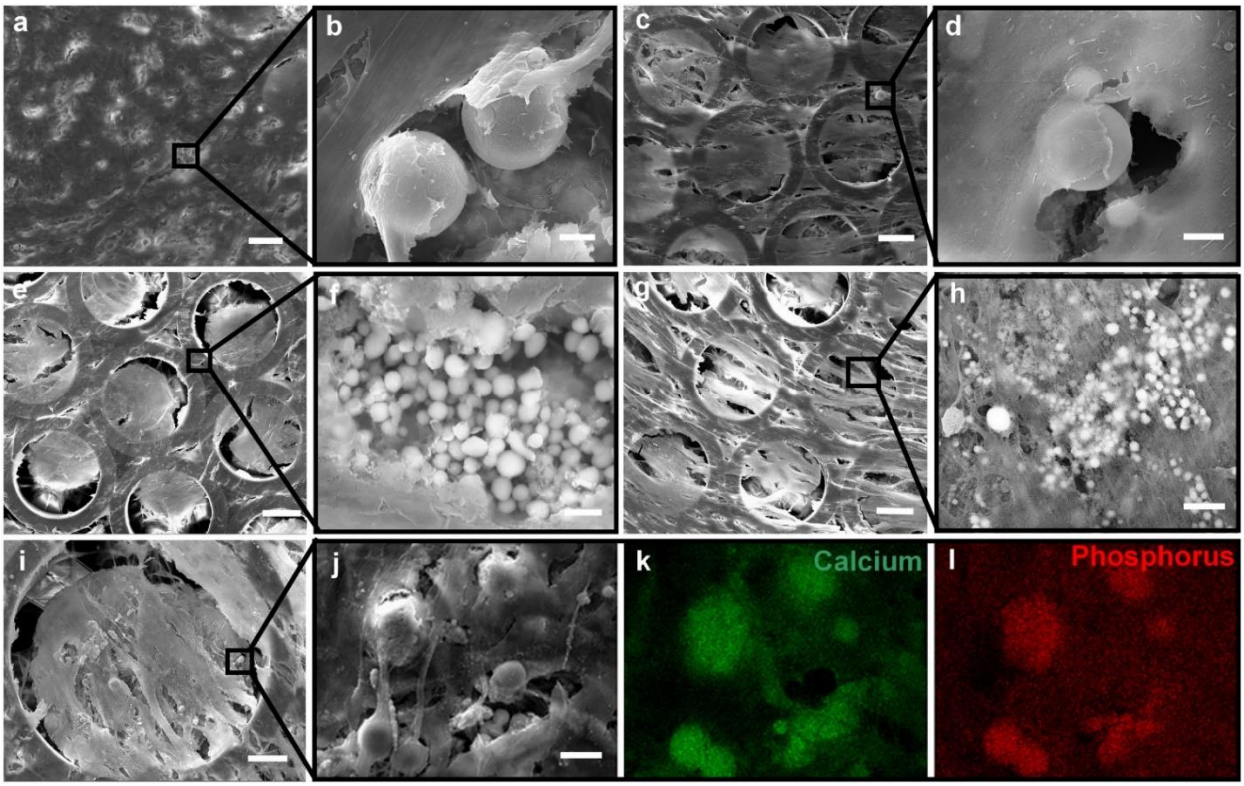

Figure 1. High magnification images showing calcium phosphate deposits of hASCs and hBMSCs cultured on Zr-Si scaffolds in osteogenic (b and d) and control (f and h) conditions; (i-l) EDX mapping confirming the presence of calcium and phosphor in the accumulations. Scale bars: (a, c, e, g) 60 μm, (b, d, f, h) 5 μm, (i) 50 μm and (j-l) 10 μm. Reproduced from Koroleva A, Deiwick A, Nguyen A, Schlie-Wolter S, Narayan R, Timashev P, Popov V, Bagratashvili V, Chichkov B. Osteogenic differentiation of human mesenchymal stem cells in 3-D Zr-Si organic-inorganic scaffolds produced by two-photon polymerization technique. PloS one. 2015;10(2):e0118164.

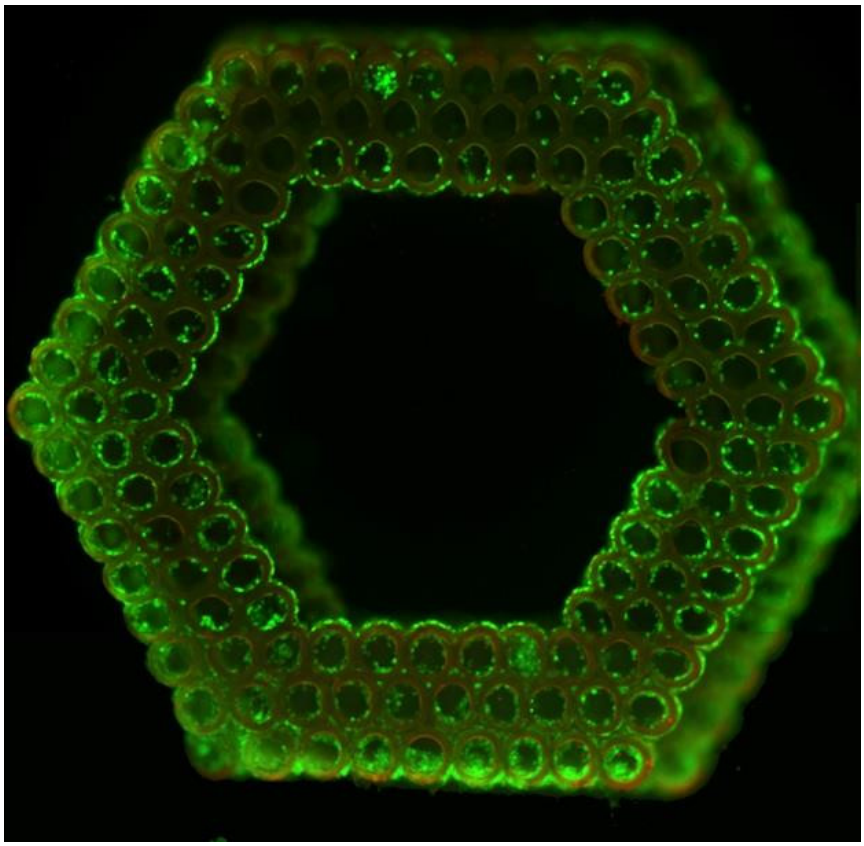

Figure 2. Live/dead staining images of 50% PEGda-riboflavin-TEOHA scaffold that was seeded with GM7373 bovine aortic endothelial cells. Live cells appear green and dead cells appear red. Due to autofluorescence, PEGda appears red. Reproduced from Nguyen AK, Gittard SD, Koroleva A, Schlie S, Gaidukeviciute A, Chichkov BN, Narayan RJ. Two-photon polymerization of polyethylene glycol diacrylate scaffolds with riboflavin and triethanolamine 2 used as a water-soluble photoinitiator. Regenerative Medicine. 2013;8:725-738.

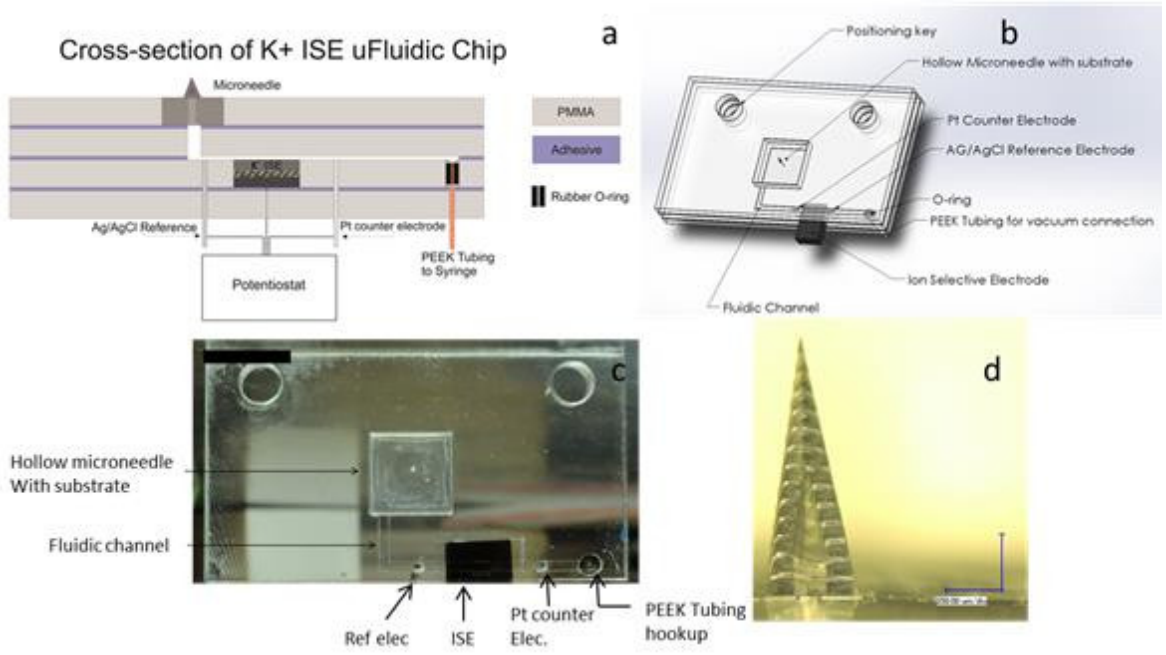

Figure 3. CorelDraw rendering of a cross-section of the K^+ ion-sensitive electrode microfluidic chip (a), solidworks drawing of K^+ ion-sensitive electrode microfluidic microfluidic chip (b), image of microfluidic chip (c) with on chip reference and counter electrodes (scale bar=10 mm) and optical image of single hollow microneedle (d) made with two-photon lithography (scale bar=250 μm). Reproduced from Miller PR, Xiao X, Brener I, Burckel DB, Narayan R, Polsky R. Microneedle-based transdermal sensor for on-chip potentiometric determination of K.+. Advanced Healthcare Materials. 2014;3:876-881 with permission of John Wiley & Sons.

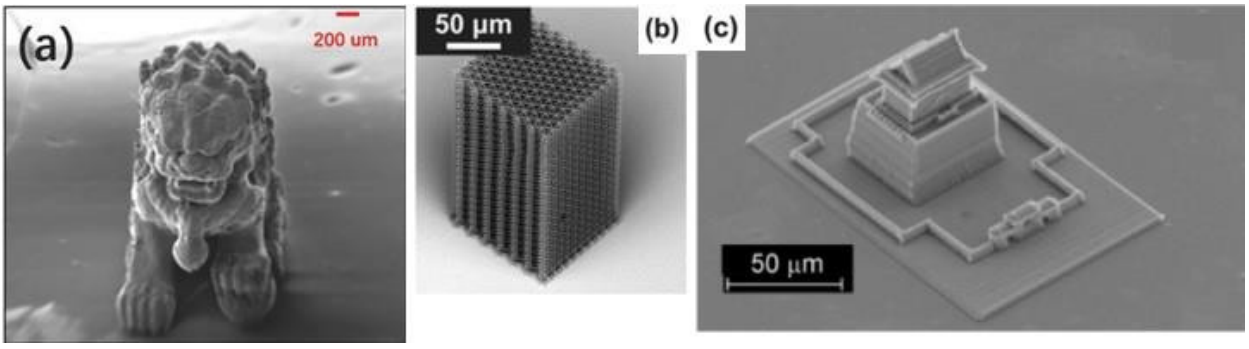

Figure 4. SEM images of representative microstructures fabricated by TPP using the methodologies described in the text. (a) SEM image in the front view of the fabricated 2 mm height lion sculpture, which was made possible by means of simultaneous spatiotemporal focusing. Reproduced from Chu W, Tan Y, Wang P, Xu J, Li W, Qi J, Cheng Y. Centimeter-Height 3D Printing with Femtosecond Laser Two-Photon Polymerization. Advanced Materials Technologies. 2018;3:1700396 with permission of John Wiley & Sons. (b) Oblique-view electron microscopy image of a mechanical metamaterial with six-fold axis on a glass substrate, which was produced by dip-in direct laser writing. Reproduced from Bückmann T, Stenger N, Kadic M, Kaschke J, Frölich A, Kennerknecht T, Eberl C, Thiel M, Wegener M. Tailored 3D mechanical metamaterials made by dip-in direct-laser-writing optical lithography. Advanced Materials. 2012;24:2710-4 with permission of John Wiley & Sons. (c) Reproduction of an ancient tower fabricated at a speed of 8 cm/s using rationally designed two-photon initiators with high polymerization efficiency. Reproduced from Li Z, Pucher N, Cicha K, Torgersen J, Ligon SC, Ajami A, Husinsky W, Rosspeintner A, Vauthey E, Naumov S, Scherzer T. A straightforward synthesis and structure–activity relationship of highly efficient initiators for two-photon polymerization. Macromolecules. 2013;46(2):352-61 with permission of the American Chemical Society.

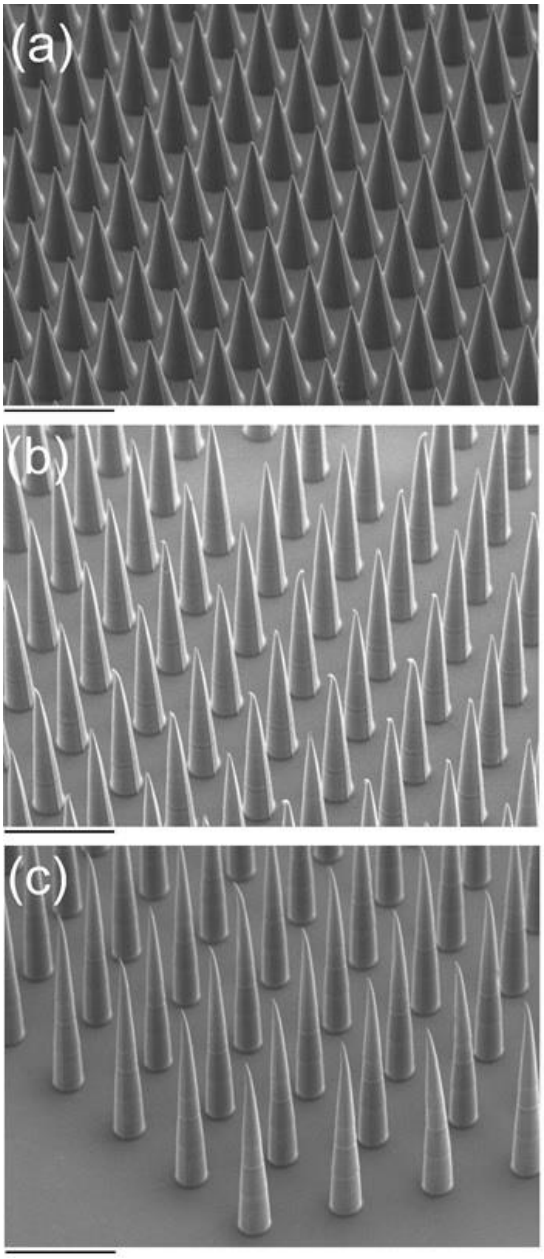

Figure 5. Scanning electron microscopy images of microneedles with nominal heights of 500 μm (*Panel A*), 750 μm (*Panel B*), and 1000 μm (*Panel C*) obtained at a stage tilt angle of 45º. The scale bars for these images are 500 μm. Reproduced from Nguyen AK, Yang KH, Bryant K, Li J, Joice AC, Werbovetz KA, Narayan RJ. Microneedle-based delivery of amphotericin B for treatment of cutaneous leishmaniasis. Biomedical Microdevices. 2019;21:8 with permission of Springer Nature.

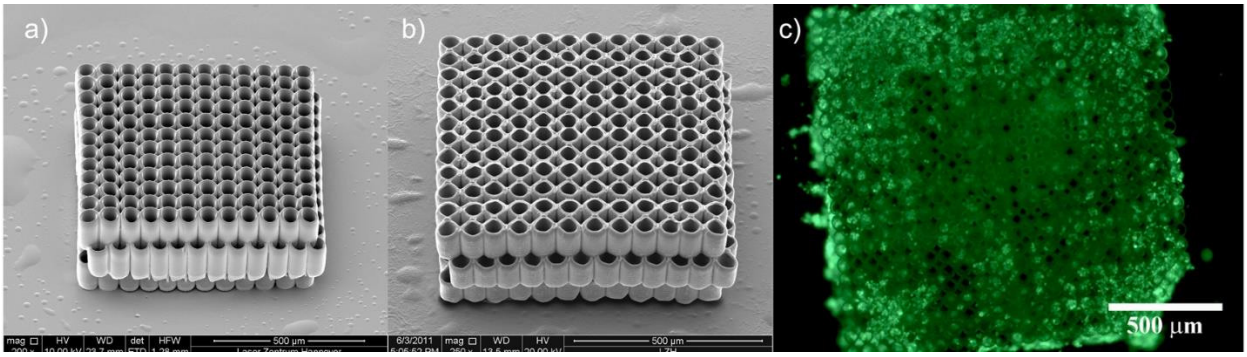

Figure 6. Tissue engineering scaffolds made by 2PP with single focus structuring (a) and four foci structuring (b). Image of bovine endothelial cells growing on a scaffold made by multibeam 2PP (c). Reproduced from Gittard SD, Nguyen A, Obata K, Koroleva A, Narayan RJ, Chichkov BN. Fabrication of microscale medical devices by two-photon polymerization with multiple foci via a spatial light modulator. Biomedical Optics Express. 2011;2:3167-3178.

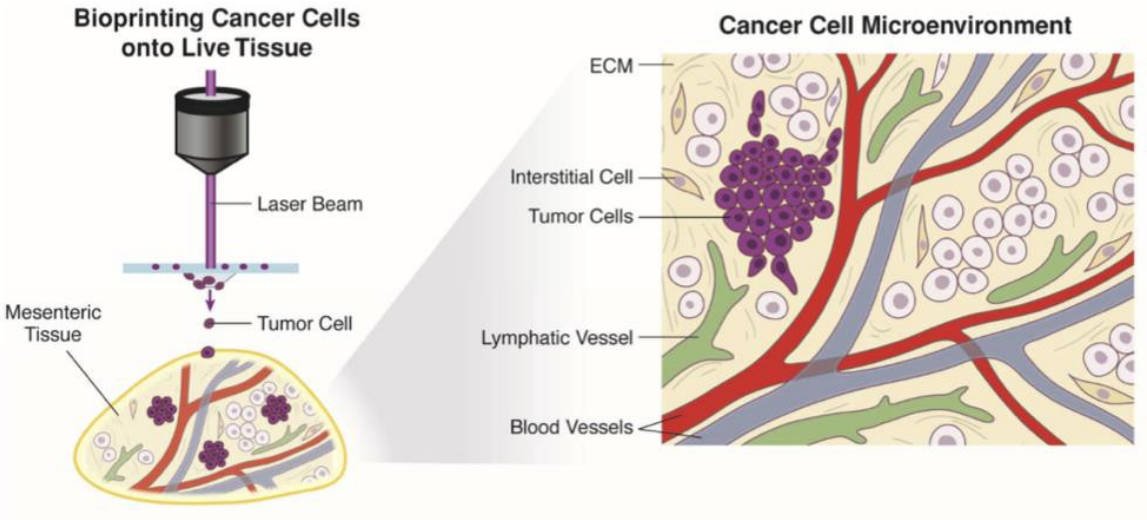

Figure 7. By combining advantages of laser direct-write and the rat mesentery culture model, cancer cells can be spatially patterned onto intact tissues and cultured. This new *ex vivo* model platform enables time lapse quantification of cancer cell behavior in an intact microvascular network environment with blood vessels, lymphatic vessels, extracellular matrix components and interstitial cells. Reproduced from Burks HE, Phamduy TB, Azimi MS, Saksena J, Burow ME, Collins-Burow BM, Chrisey DB, Murfee WL. Laser direct-write onto live tissues: a novel model for studying cancer cell migration. Journal of cellular physiology. 2016;231(11):2333-8 with permission of John Wiley & Sons.

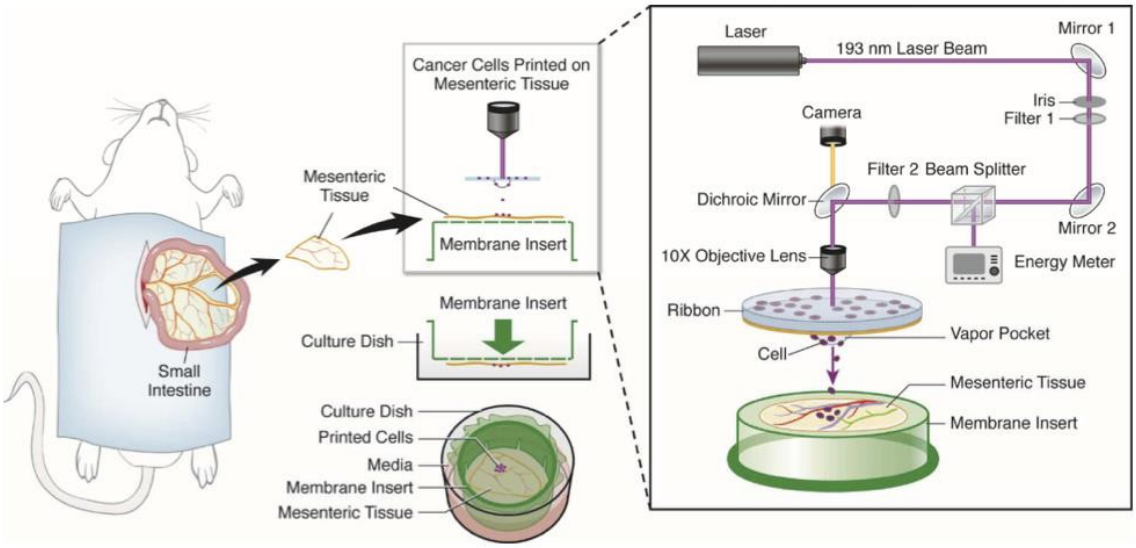

Figure 8. Rat mesenteric tissue windows, defined as the thin, translucent connective tissue section between artery/vein pairs feeding the small intestine, are harvested from adult rats and spread onto inverted commercially available trans-well inserts. Cells are then embedded in a gelatin-coated UV-transparent quartz "ribbon" can be printed directly onto the tissue. A single pulse of 193 nm ArF excimer laser causes the formation of a local vapor pocket that ejected a desired amount of cells. Use of an *in situ* camera enables real time targeting of cells. We have demonstrated that bioprinted tissues can be cultured using normal culture conditions for at least up to 5 days. Reproduced from Burks HE, Phamduy TB, Azimi MS, Saksena J, Burow ME, Collins-Burow BM, Chrisey DB, Murfee WL. Laser direct-write onto live tissues: a novel model for studying cancer cell migration. Journal of cellular physiology. 2016;231(11):2333-8 with permission of John Wiley & Sons.

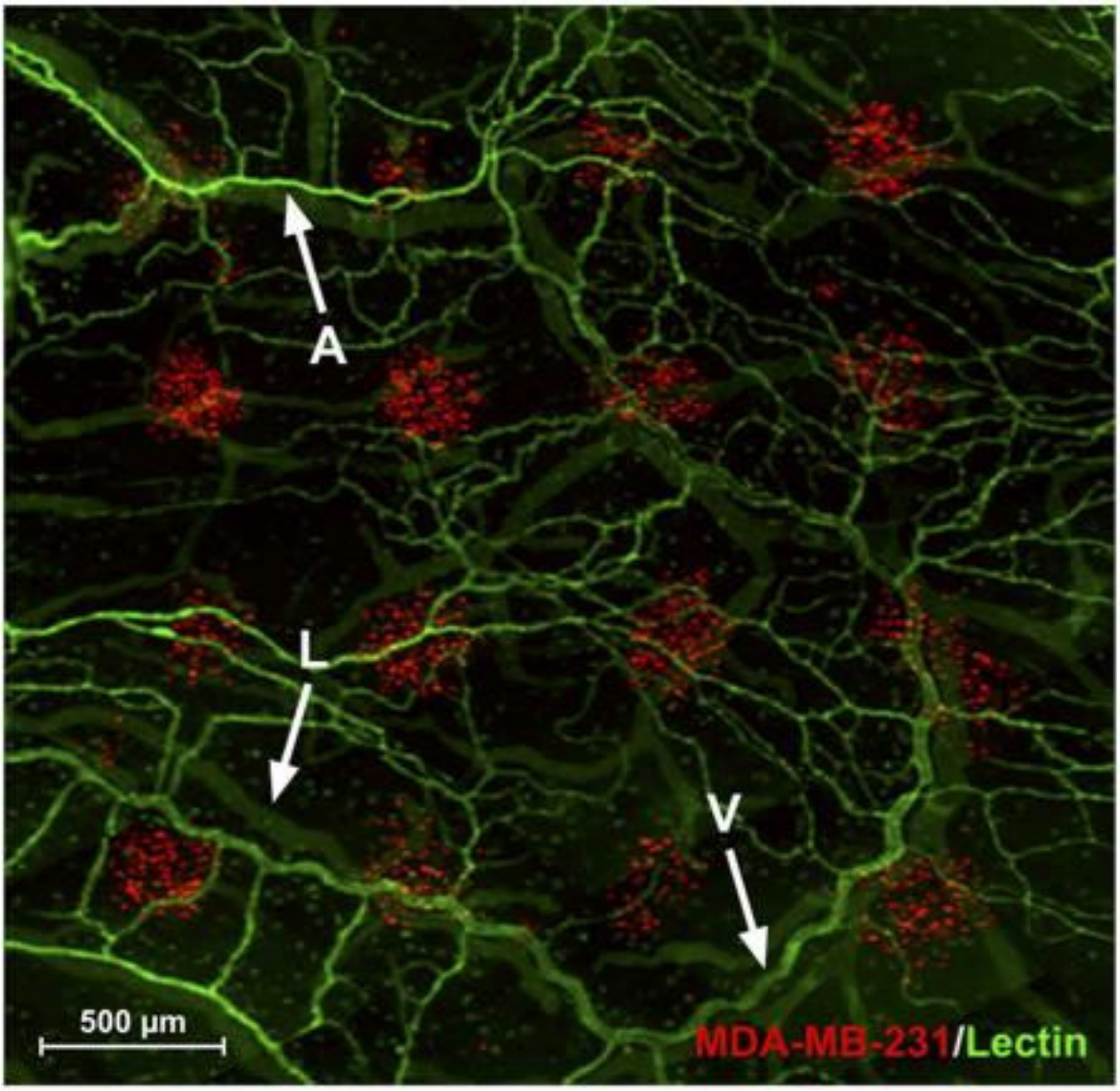

Figure 9. A) Spatially defined patterns of localized cell groups on mesentery tissue and single-cell printing capability. (A) 4 x 4 array pattern (center-to-center spacing, $d_{spacing}$ = 0.8 mm) of circular 'spots' of CellTracker Red (CTR)-labeled MDA-MB-231 cancer cells on vascularized mesentery tissue, imaged two hours following laser direct write. Mesenteric arterioles (A), venules (V), and lymphatic vessels (L) were readily identifiable by lectin labeling. Reproduced from Phamduy TB, Sweat RS, Azimi MS, Burow ME, Murfee WL, Chrisey DB. Printing cancer cells into intact microvascular networks: a model for investigating cancer cell dynamics during angiogenesis. Integrative Biology. 2015;7(9):1068-78 with permission of Oxford University Press.

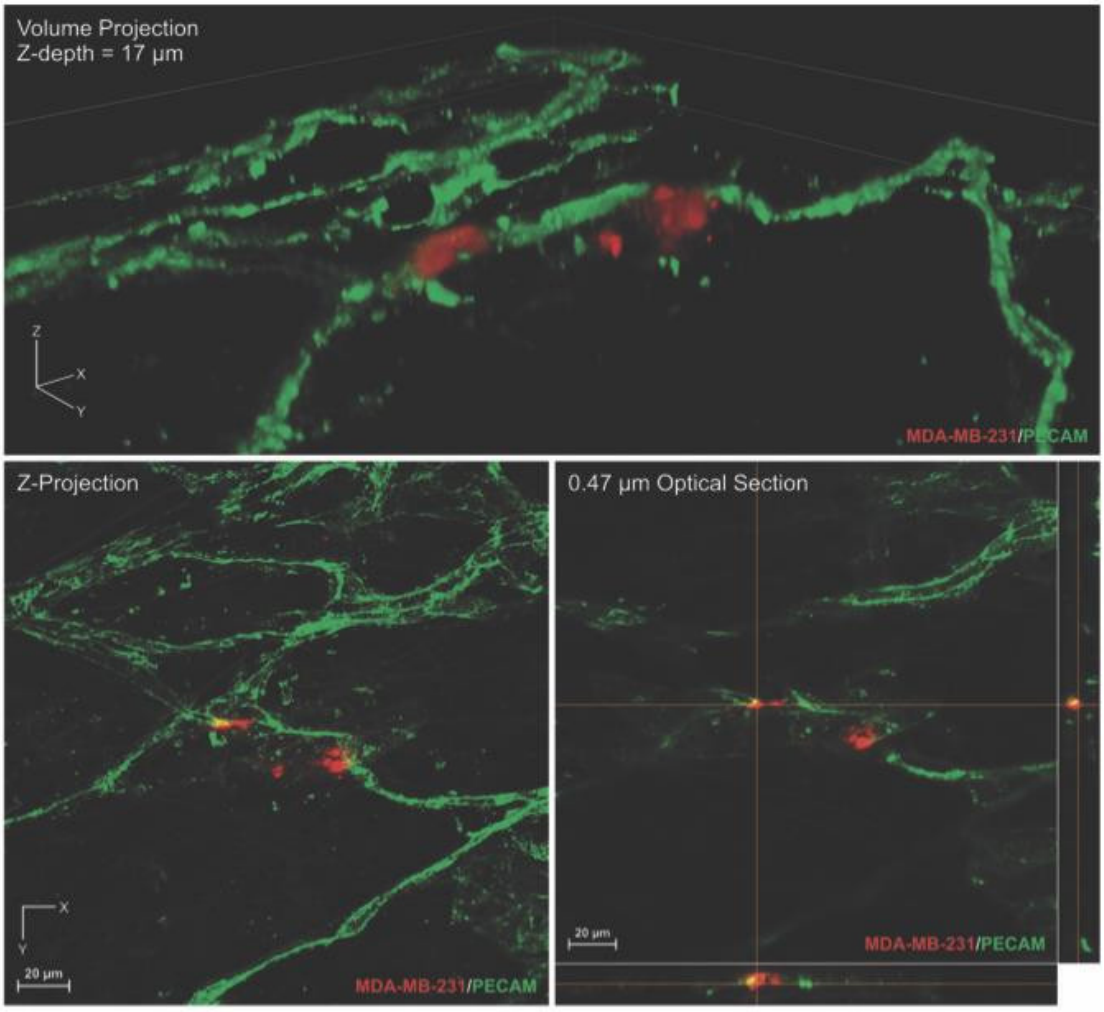

Figure 10. Interactions between cancer cells and microvascular networks are shown. MDA-MB-231 cells were identified interacting and integrating with blood vessels by using sub- micron confocal microscopy. Reproduced from Phamduy TB, Sweat RS, Azimi MS, Burow ME, Murfee WL, Chrisey DB. Printing cancer cells into intact microvascular networks: a model for investigating cancer cell dynamics during angiogenesis. Integrative Biology. 2015;7(9):1068-78 with permission of Oxford University Press.

Tommaso Baldacchini is a project scientist in the chemistry department at the University of California Irvine. He teaches physical chemistry and optics as adjunct faculty at Chapman University. He received a Ph.D. in chemistry from Boston College in 2004. From 2004 to 2006, he was a postdoctoral research fellow in the division of engineering and applied sciences at Harvard University. From 2006 to 2018, he worked as a principal scientist at Newport Corporation. His research interests focus on high-resolution laser microfabrication using ultrashort pulsed lasers.

Jayant Saksena is a biomedical engineering doctoral candidate and research assistant in the Chrisey Research Laboratory at Tulane University. He has master's degrees in bioengineering and material- and nano-science from University College Dublin and Université Pierre et Marie Curie-Sorbonne, respectively. His research involves developing bioengineered systems using laser bioprinting and processing techniques to elucidate cellular dynamics in the context of cancer and other pathologies.

Benjamin T. Vinson is a doctoral candidate and research assistant in the Chrisey Research Laboratory at Tulane University in biomedical engineering. He received his MS degree in biology from Texas Christian University, and his BS degree in biology and neuroscience from Washington and Lee University. His research focuses on fabricating microphysiological systems via laser direct-write bioprinting.

Charlie Sklare is an engineer at Medtronic working on laser-based brain therapies. He recently graduated with an interdisciplinary PhD in Physics and Math and an MS in Computational Science. His research interests are laser-based therapies, laser based bioprinting, and laser-material interaction modeling.

Yong Huang is Professor of Mechanical Engineering at the University of Florida. He received his Ph.D. from Georgia Institute of Technology. His current research interests include 3D printing of biological and engineering structures (using ink jetting, laser-induced forward transfer, and extrusion), precision machining, intelligent manufacturing.

Doug Chrisey is the Jung Professor of Materials Engineering in the Physics and Engineering Physics Department at Tulane University. He received his Ph.D. from the University of Virginia. His current research interests include photonic processing of electronic materials and tissue engineering.

Roger Narayan is a Professor in the Joint Department of Biomedical Engineering at the University of North Carolina and North Carolina State University. He received a Ph.D. from North Carolina State University and an M.D. from Wake Forest University. He currently serves as an editorial board member for several academic journals, including as editor-in-chief of Medical Devices & Sensors (Wiley) and associate editor of Applied Physics Reviews (AIP Publishing). Dr. Narayan has also edited several books, including the textbook Biomedical Materials (Springer), the handbook Materials for Medical Devices (ASM International), and The Encyclopedia of Biomedical Engineering (Elsevier). He has previously served as director of the TMS Functional Materials Division and the ASM International Emerging Technologies Awareness Committee; he currently serves as chair of the American Ceramic Society Bioceramics Division.